Applied Thermal Engineering 114 (2017) 1203–1212

Contents lists available at ScienceDirect

Applied Thermal Engineering

journal homepage: www.elsevier.com/locate/apthermeng

Research Paper

# MHD natural convection flow in a liquid metal electrode

Alberto Beltrán

*Instituto de Investigaciones en Materiales, Unidad Morelia, Universidad Nacional Autónoma de México, Antigua Carretera a Pátzcuaro No. 8701, Col. Ex Hacienda de San José de la Huerta, C.P. 58190, Morelia, Michoacán, Mexico*

## HIGHLIGHTS

- Natural convection in a LME displays the typical Bénard cells.
- The flow organizes due to the Lorentz force.
- Ohmic heating also contributes to changes in the flow.
- Good agreement is observed between numerical and the reported experimental results.

## GRAPHICAL ABSTRACT

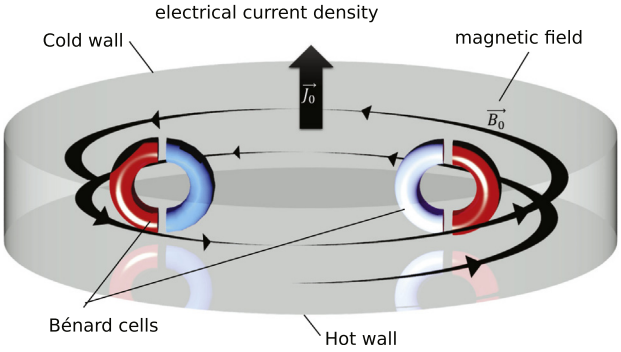


## ARTICLE INFO

*Article history:*
Received 28 January 2016
Revised 29 August 2016
Accepted 2 September 2016
Available online 6 September 2016

*Keywords:*
Natural convection
Liquid metal electrode
Lorentz force
Liquid metal battery

## ABSTRACT

The liquid metal battery is a novel grid-scale electricity storage technology; it operates at elevated temperature and consists of three horizontal liquid layers in stable density stratification. Due to the elevated temperature to keep the batteries liquid, thermal convection appears, also, during the charging/discharging processes a large electrical current density interacts with its own magnetic field generating a Lorentz force that induces motion in the stratified system. In this article, the natural convection in a liquid metal electrode (LME) candidate for LMBs is studied from a numerical point of view. Additionally, it is of interest to investigate the effect of the electrical current density on the natural convection through the Lorentz force, whose effect is called MHD natural convection. The mathematical modelling for this problem involves the solution of mass, momentum, energy and electromagnetic equations for an incompressible, viscous and electrically conducting fluid. A 3D numerical solution is implemented using the open source CFD library OpenFOAM. Numerical results indicate that the convective flow organizes due to the current. Results are compared as far as possible with experimental data.



## 1. Introduction

The growing role of renewable energy to satisfy the energy demand and its intermittent nature associated to the fact that the power grid was designed around the concept of large and controllable electric generators drive one to conclude that an important enabler for a sustainable energy future is the ability to store vast quantities of energy for grid servicing and intermittents enabling. Batteries have long been considered strong candidate solutions owing to their small spatial footprint, mechanical simplicity and flexibility in siting [1]. Recently, a novel technology has been proposed: the liquid metal battery (LMB) [2,3]; designed for storing large amounts of energy coming from renewable sources, such as wind, solar, and tidal power.

The combinations of materials and features of the currently pursued designs for the LMBs can be found in the work by Arguss [4] and Wang et al. [5]. In a simplified way a LMB can be viewed as a cylindrical container filled with three liquid layers in stable den-

*E-mail address:* albem@iim.unam.mx

http://dx.doi.org/10.1016/j.applthermaleng.2016.09.006
1359-4311/

sity stratification; in the configuration proposed by Bradwell et al. [2], they used antimony (Sb) at the bottom layer, magnesium (Mg) at the top layer and a molten salt electrolyte layer ($MgCl_2$—KCl—NaCl) in the middle, see Fig. 1. During the charging and discharging, strong electrical current density (up to 2000 A $m^{-2}$) flows between the top and bottom walls serving as current collectors. The sidewalls are electrically insulating.

The LMB technology is designed to operate at elevated temperature to keep the layers in liquid state. Adjacent layers are immiscible in each other and they swell or shrink as ions pass between them, storing or releasing energy; because everything is liquid, there is nothing that could crack after thousands of cycles, as solid electrodes might. The liquid-liquid interfaces show very fast charge transfer kinetics facilitating high current and power densities [6]. Additionally, since the LMBs are virtually self-assembling, they allow for an extremely simple and therefore cost-efficient design [7] increasing their attractiveness for stationary applications.

Transferring the attractive concept to an industrial scale means to first understand and then address a number of issues mainly rooted in fluid mechanical instabilities. These instabilities can destroy the stable density stratification thereby causing battery failure. Depending on the batterie's cross section, which is determined by the achievable current density and the projected charge/discharge time; LMBs can be classified in two types: tall and shallow cells, in each one different instabilities will occur. Tall cells are most susceptible to a Magnetohydrodynamic (MHD) phenomenon, the Tayler instability (TI) [8–11]. On the other side, shallow cells are dominated by the interfacial regions; it is to be expected that interface instabilities related to those observed in aluminum reduction cells (ARCs) have to be taken into account [12–14].

This work presents the numerical research on the MHD natural convection flow in a layer of the eutectic alloy of lead and bismuth (*ePbBi*) studied by Kelley and Sadoway [15] as a good liquid metal electrode (LME) candidate for the LMBs. Essentially in their experimental configuration, the flow can be driven by various processes. First, keeping the LME liquid requires maintaining elevated temperatures and unavoidably introduces thermal gradients and therefore natural convection. Second, this electrode accommodates a large electrical current (from 0 to 4000 A $m^{-2}$) which interacts with its own magnetic field generating a Lorentz force (MHD effect) that modifies the mixing flow behavior. Additional thermal gradients can arise locally from ohmic and entropic heating. Previous transport phenomena are studied from a numerical point of view and the obtained results are compared as far as possible with experimental data.

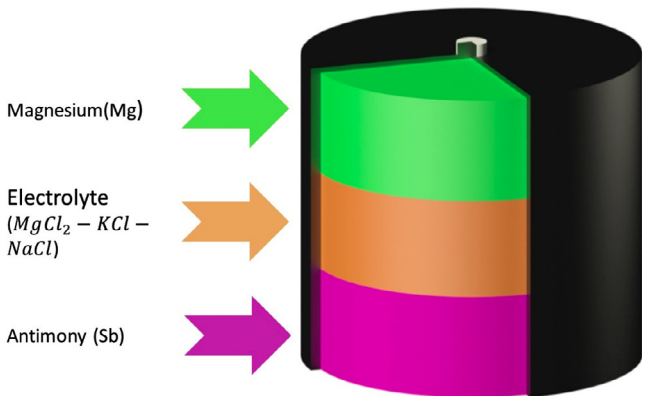


**Fig. 1.** Sketch of the LMB prototype developed by Bradwell et al. [2].

The paper is organized as follows. In Section 2, we describe the physical model under study. In Section 3 we provide a brief description of the MHD natural convection flow and the assumptions under which our problem will be set, including all the governing equations and boundary conditions. This is followed in Section 4 with the numerical results as well as some discussions are presented. The paper is closed in Section 5 with concluding remarks.

## 2. Physical model

This study is focused on the flow behavior into a LME, a key component of the LMBs. Actually, very few experimental work has been done on this kind of configurations under designs and operating conditions viable for commercial development. In particular, it is of interest the work by Kelley and Sadoway [15]; where they built an experimental LME prototype, it consists of a *ePbBi* positive electrode confined in a stainless steel cylindrical vessel which also serves as a positive current collector, maintaining electrical contact with the (liquid) positive electrode and thereby allowing current flow to a load or supply. A separate negative current collector, made of nickel-iron foam, provides the second terminal. To hold the *ePbBi* near 423 K the vessel is heated from below through copper plate and insulated around its sides, see Fig. 2.

The authors consider a temperature difference along the LME of $\Delta T = 10$ K; in our case we define such difference as $\Delta T = T_H - T_C$, where $T_C$ and $T_H$ are the cold and hot temperatures on the top and bottom walls, respectively. By using an ultrasound probe connected to Ultrasonic Dopler Velocimeter equipment (UDV) they measured velocity profiles in the radial direction. The diameter, $D$, ($x$—$z$ plane) and height, $L$, ($y$-direction) of the LME are: $D = 8.89 \times 10^{-2}$ m and $L = 1.6 \times 10^{-2}$ m, respectively.

Experimental velocity measurements without currents indicate that the flow is driven by natural convection and since $L$ is small compared to $D$; the typical Bénard cells are expected to be observed. In particular, from the UDV measurements up to four vortices distributed in the radial direction can be observed. When a direct electrical current density is injected in the LME, experimental measurements show that the convective flow organizes in a different way. Fig. 3 illustrates the expected flow pattern and the directions of the applied direct electrical current density and its associated static magnetic field, simulating the charging process for the LMBs.

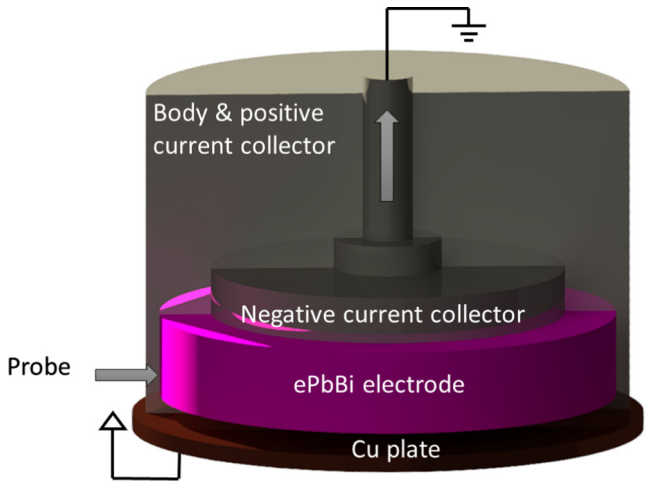


**Fig. 2.** Sketch of LME experimental configuration studied by Kelley and Sadoway [15].

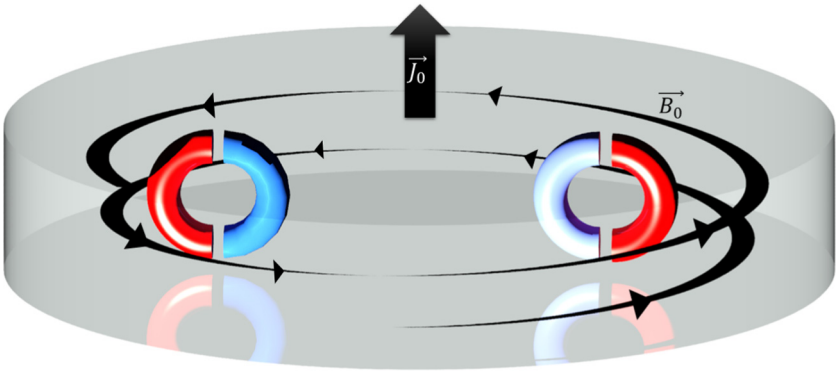


**Fig. 3.** Sketch for the expected convective flow pattern due to $\Delta T$; as well as, the directions for the applied direct electrical current density, $\vec{j}_0$ and its associated static magnetic field, $\vec{B}_0$ in the LME configuration studied by Kelley and Sadoway [15].

Due to the high temperature at which the experiments are conducted, very few physical variables can be measured in the previously described system. Experimentally only de temperature difference, $\Delta T$, and velocity profiles along the radial direction are reported. On the other side, mathematical modelling and 3D numerical simulations (under certain assumptions) are capable to address multiple physical effects and to obtain values for the variables in the whole domain; in fact, through the numerical study of the LME, it is possible to study hydrodynamic and thermal variables like velocity and temperature fields, respectively; as well as, electromagnetic variables like the electric potential and the induced electrical current density. Through the study of these variables and its interactions, it is possible to understand the hydrodynamic and thermal behavior. Next section is focused on this subject.

## 3. Mathematical model

Even in its simplified form the LME is a complex electro-magneto-hydrodynamic system. Assuming the *ePbBi* eutectic alloy as a Newtonian, incompressible and electrically conducting fluid, the dynamics and heat transfer (using the Boussinesq approximation) in the LME can be described by the mass conservation, Navier-Stokes, energy and electromagnetic equations:

$$\nabla \cdot \vec{U} = 0 \tag{1}$$

$$\frac{\partial \vec{U}}{\partial t} + \left(\vec{U}\cdot\nabla\right)\vec{U} = -\frac{\nabla p}{\rho} + \frac{\mu}{\rho}\nabla^2\vec{U} + \frac{(\vec{j}_{in} + \vec{j}_0)\times\vec{B}_0}{\rho} - \beta(T - T_c)g\hat{j}, \tag{2}$$

$$\frac{\partial T}{\partial t} + \left(\vec{U}\cdot\nabla\right)T = \frac{k}{\rho Cp}\nabla^2 T + \frac{j_{in}^2 + j_0^2}{\sigma\rho Cp} + \frac{\mu(\nabla\vec{U} + \nabla\vec{U}^T)\cdot\nabla\vec{U}}{\rho Cp}, \tag{3}$$

$$\vec{j}_{in} = \sigma(-\nabla\varphi + \vec{U}\times\vec{B}_0), \tag{4}$$

where $t$, $\vec{U}$, $\vec{j}_{in}$, $\vec{j}_0$ and $\vec{B}_0$ represent the time, the velocity, the induced and applied electrical current density and the static magnetic vector fields, respectively; $T$ the temperature field, $\varphi$ is the electric potential, $j_{in}$ and $j_0$ the induced and applied electrical current densities magnitude and $g$ is the gravity of Earth. The physical properties for the *ePbBi* alloy are: density $\rho$, dynamic viscosity $\mu$, electrical conductivity $\sigma$, thermal conductivity $k$, specific heat $Cp$ and thermal expansion coefficient $\beta$. Third and fourth terms in the

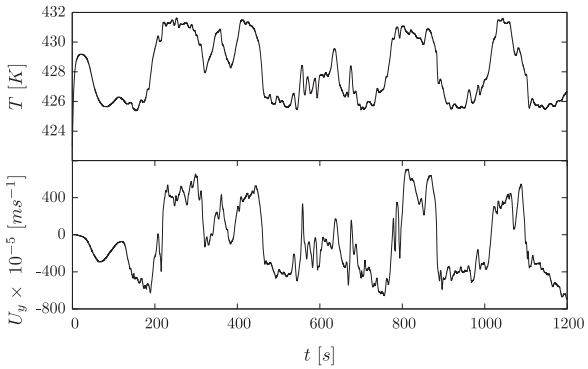


**Fig. 5.** Temperature and $U_y$ velocity component vs. time at $x = 0$, $y = 8 \times 10^{-3}$ m and $z = 0$.

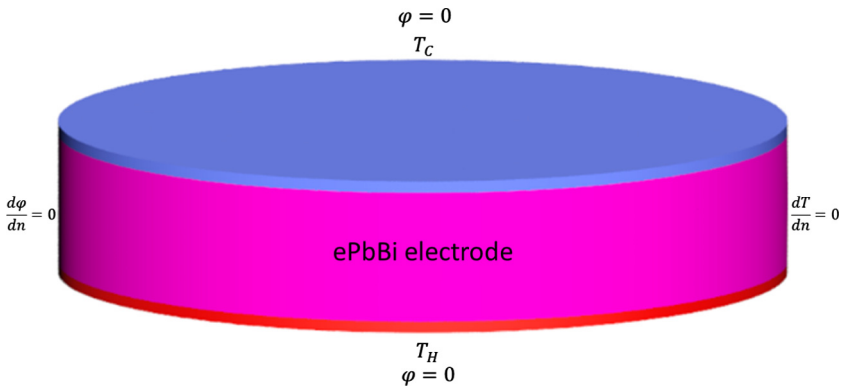


**Fig. 4.** Boundary conditions for the numerical study of the LME.

RHS of Eq. (2) represent the Lorentz and buoyancy forces, respectively; while the second and third therm in the RHS of Eq. (3) represent the volumetric heating rate due to the Joule's and viscous dissipation, respectively. The state equation for the density is $\rho = \rho_0(1 - \beta(T - T_C))$, where $\rho_0$ is the density for $T_C$. The rest of the physical properties are assumed to be constant.

Eq. (4) represents the Ohm's law for moving conductors. Applying the divergence operator to Ohms law and demanding charge conservation, $\nabla \cdot \vec{j}_{in} = 0$, we arrive at the Poisson equation for the electric potential,

$$\nabla^2 \varphi = \nabla \cdot (\vec{U} \times \vec{B}_0), \tag{5}$$

Given $j_0$ (e.g. the battery charging current) the associated static magnetic field can be calculated using:

$$\vec{B}_0(x, y, z) = \frac{\mu_0 j_0}{2}(z\hat{i} - x\hat{k}). \tag{6}$$

where $\mu_0$ is the vacuum permeability. Eq. (6) is used as a first approximation (considering the LME as an infinitely long vertical cylinder).

The boundary conditions for our LME configuration consider on the bottom wall $T = T_H$ and $\varphi = 0$; on the top wall $T = T_C$ and $\varphi = 0$; while the lateral wall is assumed to be adiabatic, $\frac{dT}{dn} = 0$, and non-conducting $\frac{d\varphi}{dn} = 0$, an explanation for the electric

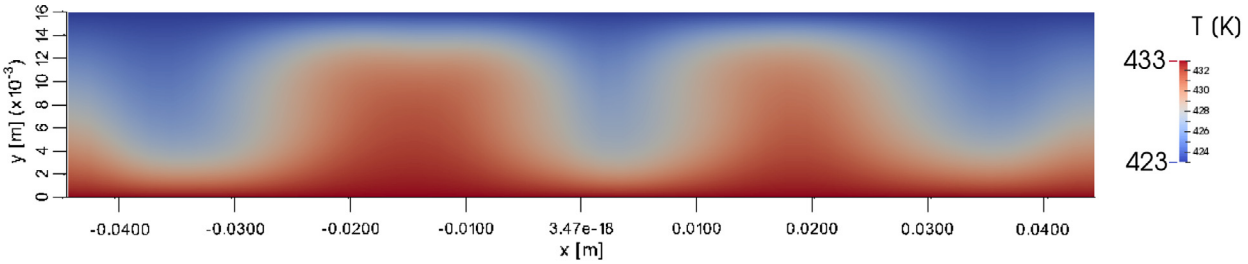


(a) Temperature field

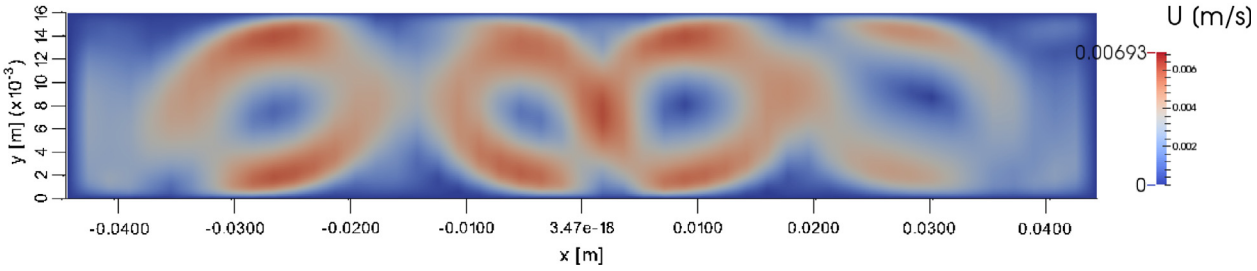


(b) Velocity magnitude

**Fig. 6.** Temperature and velocity magnitude distributions in the $x$–$y$ plane at $z = 0$, for both $j_0 = 0$ A m$^{-2}$ and $t = 1000$ s.

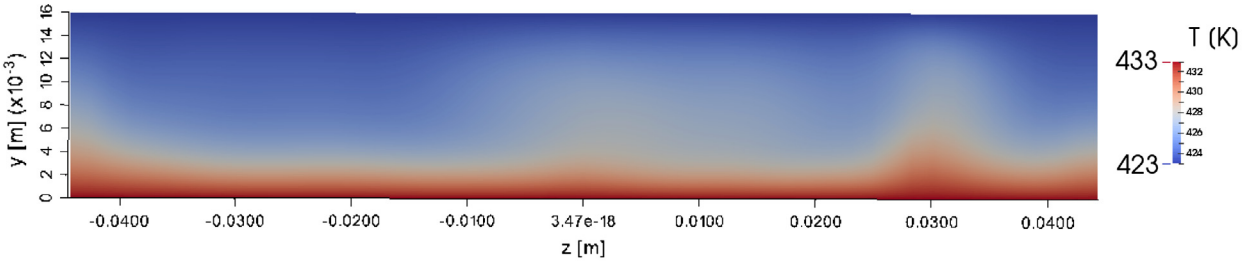


(a) Temperature field

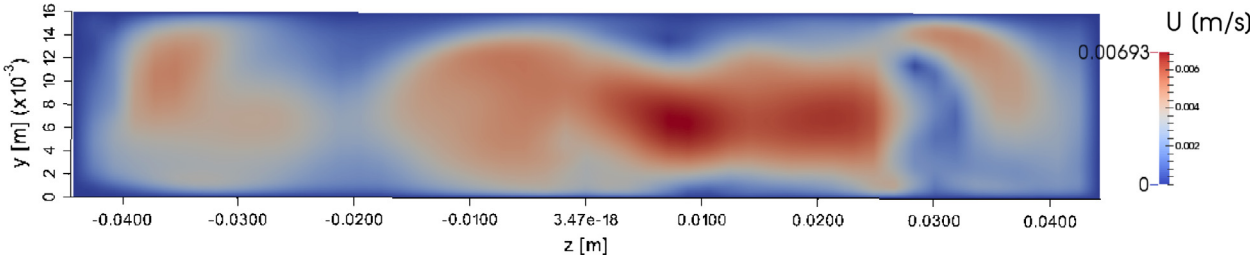


(b) Velocity magnitude

**Fig. 7.** Temperature and velocity magnitude distributions in the $z$–$y$ plane at $x = 0$, for both $j_0 = 0$ A m$^{-2}$ and $t = 1000$ s.

potential boundary conditions on the top and bottom walls can be seen in Weber et al. [11]. The no-slip condition for the velocity is assumed at all boundaries, see Fig. 4. The physical properties are kept constant (at $T_C = 423$ K): $\mu = 2.94 \times 10^{-3}$ kg/ms, $\sigma = 9.26 \times 10^5$ s$^3$ C$^2$/(m$^3$ kg), $k = 9.6$ kg m/(K s$^3$), $\beta = 4.24 \times 10^{-5}$ K$^{-1}$, $Cp = 148.76$ m$^2$/(s$^2$ K) and $\rho_0 = 10540$ kg/m$^3$, values reported by Kelley and Sadoway [15].

A 3D numerical solution is implemented using the open source CFD library OpenFOAM [16]. The coordinate system is located at the center of the vessel and at the bottom wall, the $y$ direction is

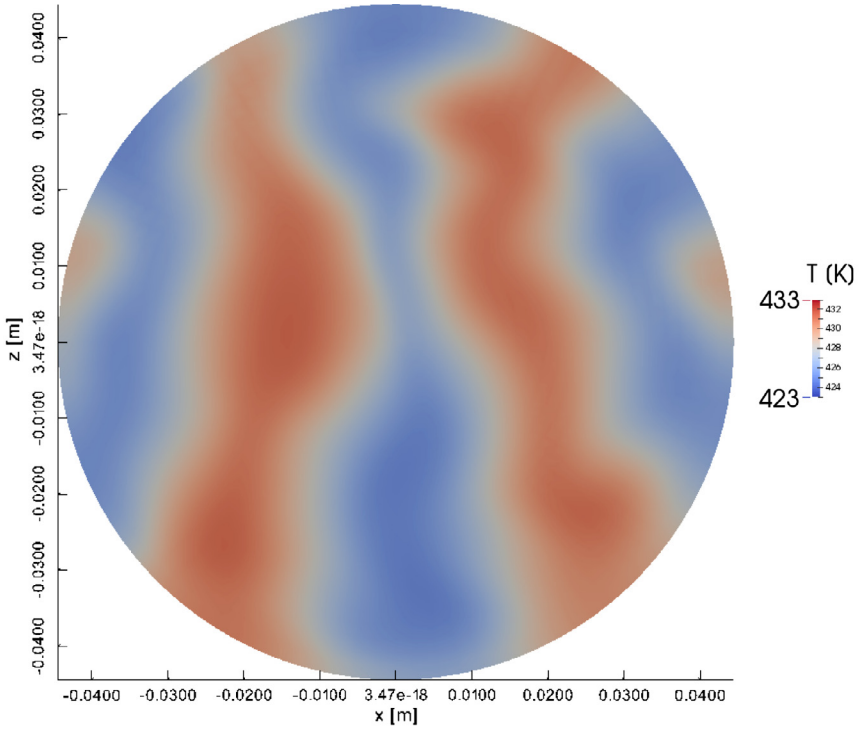


(a) Temperature field

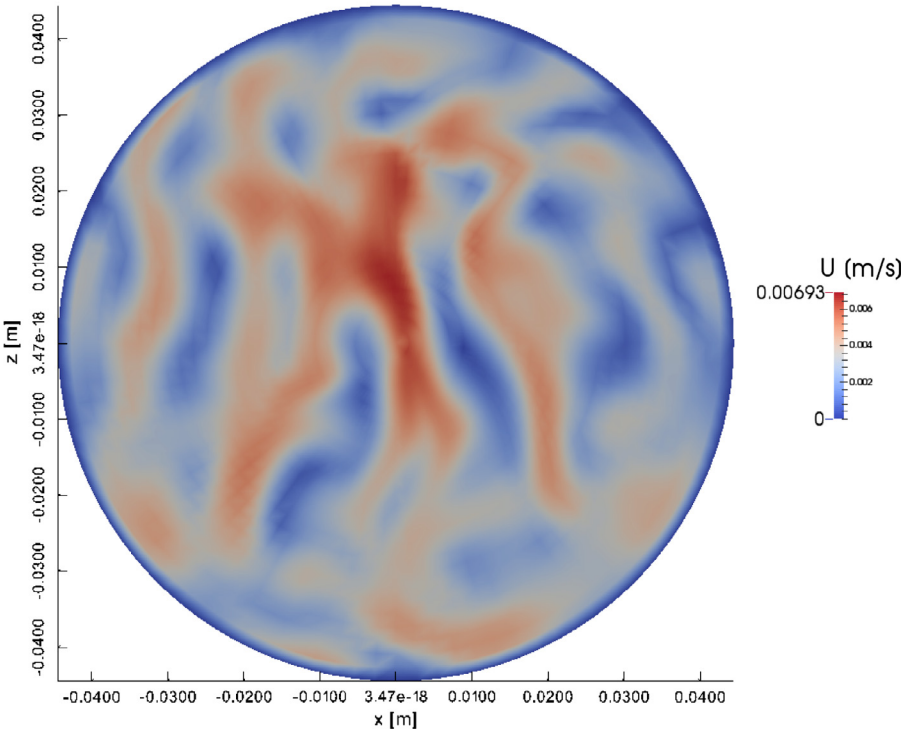


(b) Velocity magnitude

**Fig. 8.** Temperature and velocity magnitude distributions in the $x$–$z$ plane at $y = 0.08$ m, for both $j_0 = 0$ A m$^{-2}$ and $t = 1000$ s.

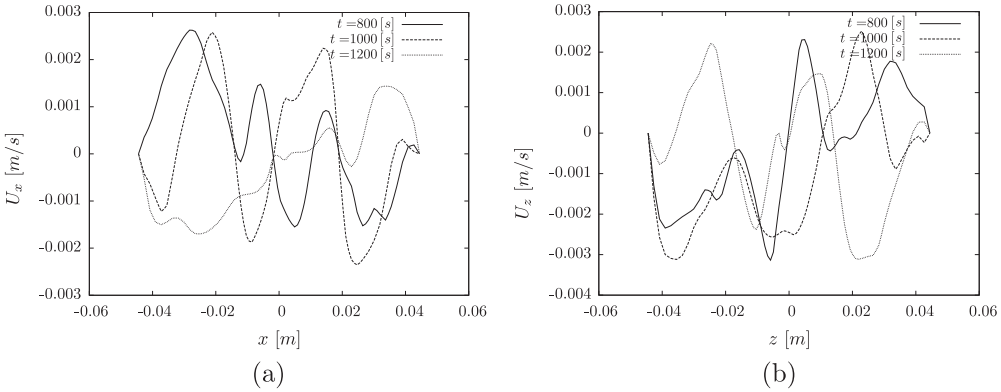


**Fig. 9.** For three different instants of time (a) $U_x$ velocity profile vs. $x$ at $y = 6 \times 10^{-3}$ m and $z = 0$; (b) $U_z$ velocity profile vs. $z$ at $y = 6 \times 10^{-3}$ m and $x = 0$.

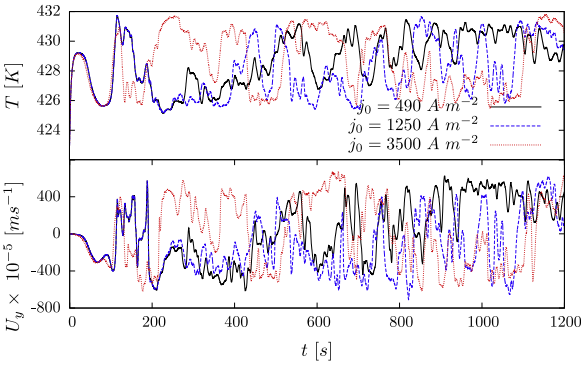


**Fig. 10.** Temperature and $U_y$ velocity component vs. time at $x = 0$, $y = 8 \times 10^{-3}$ m and $z = 0$ for $j_0 = 490$, 1250 and 3500 A m$^{-2}$.

measured along the LME width (axial direction), the $x$ and $z$ directions in the bottom wall. For all calculations, a grid of $100 \times 80 \times 100$ volume elements is used in the $x$, $y$ and $z$ direction, respectively; while for the Crank-Nicholson time-marching procedure a time step of $5 \times 10^{-3}$ s is used. Simulations run a total of $2.4 \times 10^5$ time steps; for all simulated cases, an absolute tolerance of $10^{-6}$ was fixed at each time step as convergence criteria for the mass and charge conservation.

## 4. Numerical results

The main interest is to understand from a numerical point of view the MHD natural convection flow in a LME. In order to validate our results we compare as far as possible with the experimental observations reported by Kelley and Sadoway [15]. Firstly, we analyze the isolated effect of thermal convection (without current, $j_0 = 0$), for this case, the flow is driven by just a temperature difference imposed across the top and bottom walls of the LME. In our model the Lorentz force term in Eq. (2) and the Joule's dissipation term in Eq. (3) are neglected. Experimentally the flow is assumed to be kept at $T_C = 423$ K and subject to $\Delta T = 10$ K, under these conditions a time dependent flow is observed through the UDV measurements; assuming same conditions in our simulations, a similar flow behavior is observed as depicted in Fig. 5, where measurements of the temperature field and the velocity component in the gravity direction at the mid-height of the layer are shown.

As can be seen in Fig. 6a and b, the temperature distribution, $T$, and the velocity magnitude, $U$, in the mid-planes of the LME domain clearly show the typical thermal plumes and Bénard cells, respectively. It is important to remember that since the flow is time dependent the number of vortices varies; furthermore, since the flow is 3D, a perpendicular plane to the previous one will show different structures for the temperature and velocity fields, see

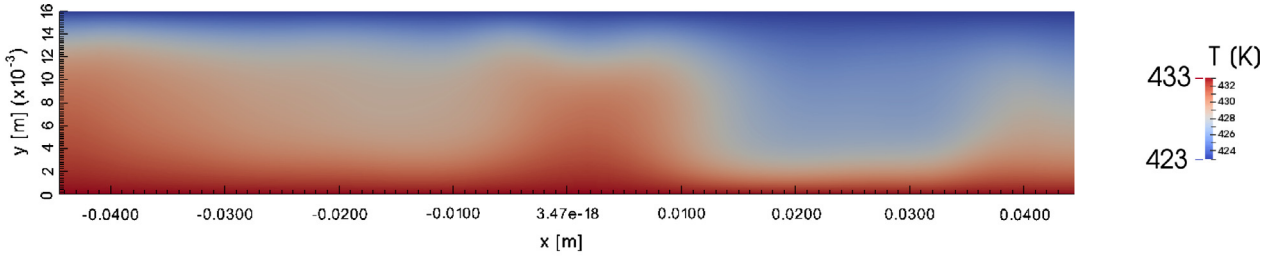


(b) Velocity magnitude

**Fig. 11.** Temperature and velocity magnitude distributions in the $x$–$y$ plane at $z = 0$, for both $j_0 = 1250$ A m$^{-2}$ and $t = 1000$ s.

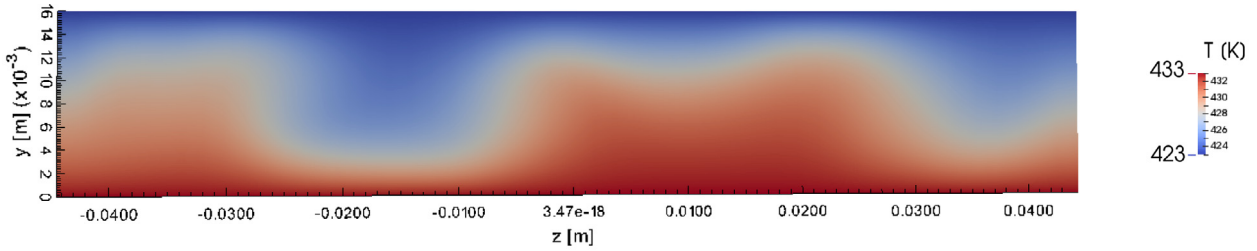


(a) Temperature field

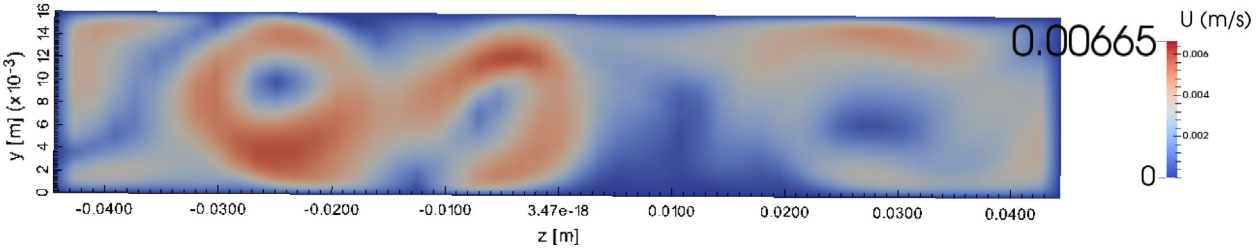


(b) Velocity magnitude

**Fig. 12.** Temperature and velocity magnitude distributions in the $z$–$y$ plane at $x = 0$, for both $j_0 = 1250$ A m$^{-2}$ and $t = 1000$ s.

Fig. 7a and b. Interestingly, in Fig. 6b up to four vortices are shown, similar number to the one reported in the experiments.

Additionally, Fig. 8a and b confirms the non-symmetrical flow behavior.

In order to compare with the experimental observations from the ultrasound probe, located slightly below half width of the LME, velocity profiles are extracted from the 3D numerical solution along the axes, they can give us information about the exact number of vortices present in the flow configuration. For three different instants of time, Fig. 9a and b shows the $U_x$ and $U_z$ velocity components along the $x$ and $z$ axes (at $y = 6 \times 10^{-3}$ m), respectively. Due to the time dependent flow behavior a direct comparison with experiments is not possible; but, interestingly numerical results are in the same order of magnitude, $10^{-3}$ m/s, and predict the same number of vortices than those reported in the experiment.

To simulate experimentally the charging/discharging processes in the LMB, an external direct electrical current density is applied in the LME, this current interacts with its own magnetic field and generates a Lorentz force that modifies the existing flow. To understand the effect of this force, numerical simulations were performed but now assuming a uniform current density in the axial direction, $\vec{j}_0 = j_0\,\hat{y}$, with a magnitude in the range of $0 < j_0 \leqslant 4000$ A m$^{-2}$, similar to the one reported in the experiments.

Results for all the current values show that the time dependent flow behavior is preserved; as an example see Fig. 10, where the temperature and $U_y$ velocity component were monitoring at the center of the LME for three different current values.

It should be pointed out that, the effect of the Lorentz force can be clearly appreciated by taking a look on the temperature and velocity distributions at different planes, for instance see Figs. 11–13 where different temperature and flow patterns for $j_0 = 1250$ A m$^{-2}$ are shown. A direct comparison with those observed without current (Figs. 6–8) shows that a small number of vortices is observed, situation that resembles a more ordered flow.

In Fig. 14a and b the velocity profiles for $j_0 < 1250$ A m$^{-2}$ are less curved than those without current, which is an additional indicator of the presence of a different number of vortices; while for $j_0 \geqslant 1250$ A m$^{-2}$ velocity profiles are similar. Additionally, in the $z$-direction slightly higher vales for $j_0 = 3500$ A m$^{-2}$ compared to $j_0 = 0$ can be seen in Fig. 14b, previous statement is in agreement with the reported experimental measurements.

Finally, to see the effect of $j_0$ on the flow and thermal patterns, the typical Nusselt number, $Nu$, is calculated at the bottom wall, the higher the $Nu$ number the better the heat transfer rate, which in the LME case is associated to the flow convection. To evaluate the $Nu$ number the following expression is used:

$$Nu = \frac{L}{T_H - T_C} \int_S \left.\frac{dT}{dy}\right|_{y=0} dS \tag{7}$$

where $S$ is the area of the bottom wall.

Based on the time dependent flow observed in all simulated cases, this $Nu$ number is a function of time, $Nu(t)$, and is calculated every 50 s for $0 \leqslant j_0 \leqslant 4000$ A m$^{-2}$ in intervals of 250 A m$^{-2}$. Fig. 15a shows the $Nu(t)$ for four different $j_0$ values.

In terms of the $Nu(t)$, a time average Nusselt number, $\overline{Nu}$, can be defined as:

$$\overline{Nu} = \frac{1}{N_t} \sum_{t=1}^{N_t} Nu(t) \tag{8}$$

where $N_t$ is the number of time intervals at which the $Nu$ was calculated for each $j_0$ value. Fig. 15b shows the $\overline{Nu}$ as a function of $j_0$. As can be seen, the higher $\overline{Nu}$ value corresponds to $j_0 = 0$, and it decreases as $j_0$ increases; however, it is important to notice that for the $2750 \leqslant j_0 \leqslant 4000$ A m$^{-2}$ interval, the $\overline{Nu}$ value increases to reach almost the same value than that for $j_0 = 0$; interestingly, in this same interval the experimental results show a slight increase in mixing time [15]. Our results would confirm that ohmic heating may also contribute to changes in the flow.

Horanyi et al. [17] report correlations for the calculation of $Nu$ for some liquid metals as a function of $Ra$ number, defined as $Ra = \rho g \beta \Delta T L^3/\mu k$; for the case of mercury:

$$Nu = 0.147 Ra^{0.257} \tag{9}$$

Previous expression is valid for $1 \times 10^3 \leqslant Ra \leqslant 5 \times 10^5$; in their experiments Kelley and Sadoway [15] report $Ra = 1 \times 10^4$, using Eq. (9) a value of $Nu = 1.5678$ is obtained, quite similar to $\overline{Nu} = 1.6948$ for $j_0 = 0$.

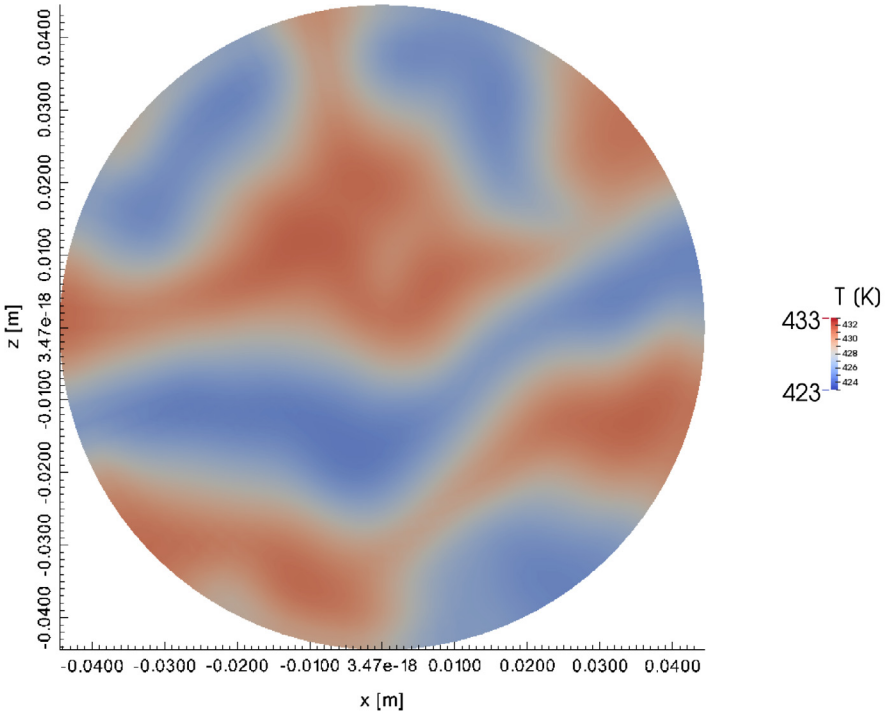


(a) Temperature field

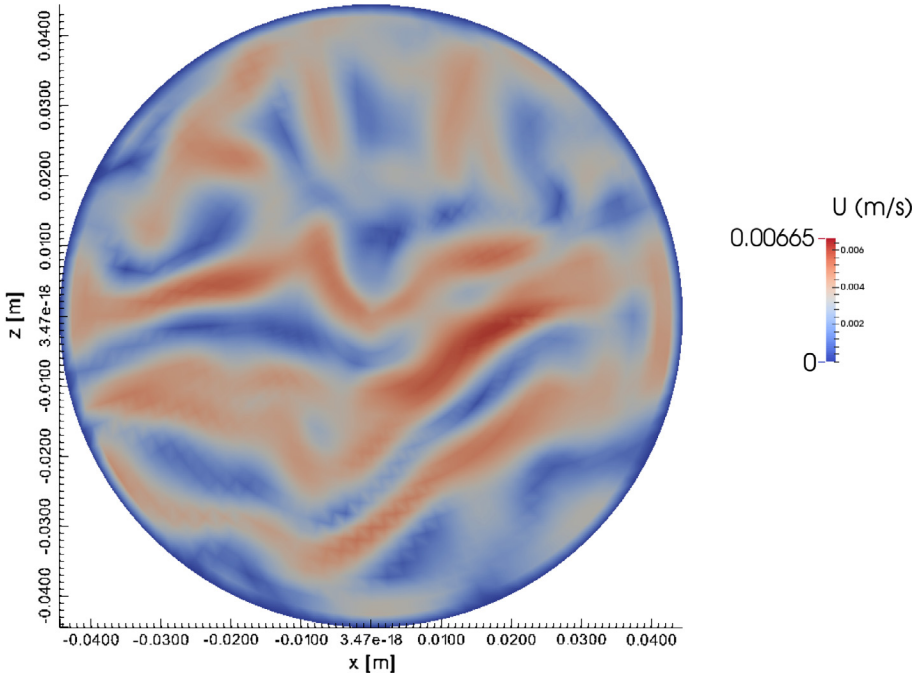


(b) Velocity magnitude

**Fig. 13.** Temperature and velocity magnitude distributions in the $x$–$z$ plane at $y = 0.08$ m, for both $j_0 = 1250$ A m$^{-2}$ and $t = 1000$ s.

It should be mentioned that the fluctuation of the *Nu* number shown in Fig. 15a is in qualitative good agreement with other reported experimental and numerical results. For instance, velocity profiles measurements performed by Kelley and Sadoway [15], indicate the presence of time dependent flow structures, situation that would imply a temperature time dependent behavior and therefore a time varying *Nu* number. On the other side, numerical simulations by Verzicco and Camussi [18] show that for a cylindrical cavity with aspect ratio (diameter/height) 1, heated from below, cooled from above and filled with mercury, several transitions from steady up to turbulent convection, passing through periodic and chaotic flow regimes are observed

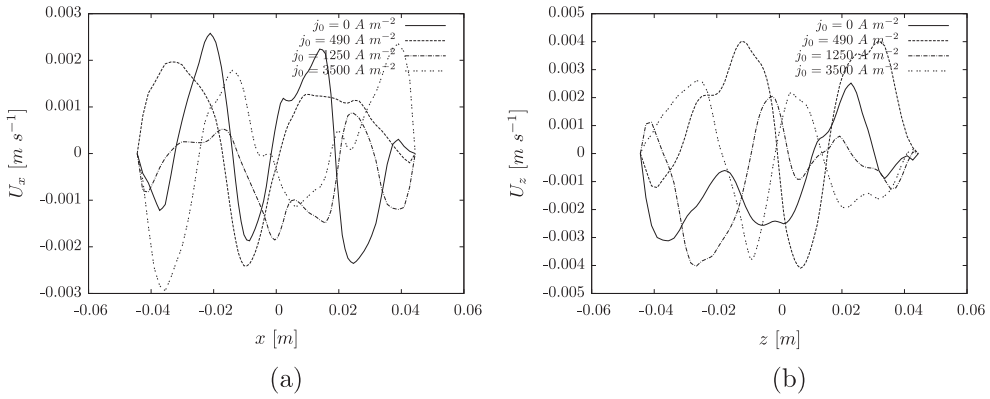


**Fig. 14.** For three different current values and $t = 1000$ s: (a) $U_x$ velocity profile vs. $x$ at $y = 6 \times 10^{-3}$ m and $z = 0$; (b) $U_z$ velocity profile vs. $z$ at $y = 6 \times 10^{-3}$ m and $x = 0$.

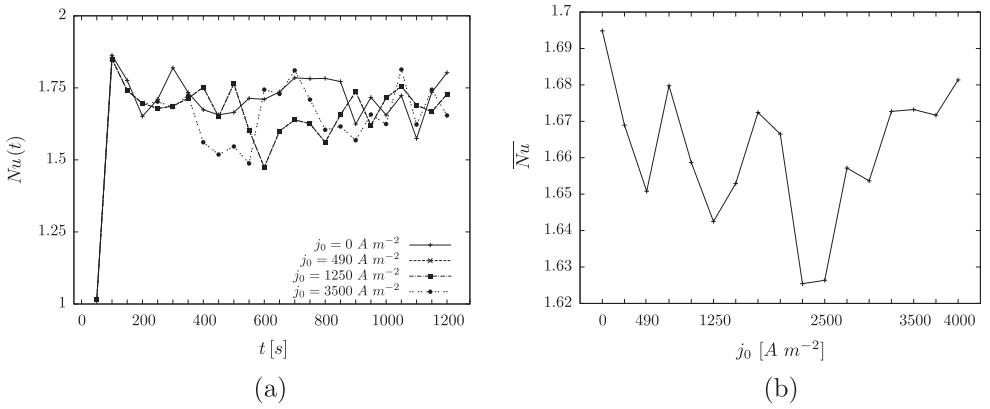


**Fig. 15.** (a) Nusselt number vs. time. Comparison for the case without and three different electrical current density values; (b) Time average Nusselt number vs. electrical current density.

depending on the *Ra* number. In particular, their calculations for the time evolution of the *Nu* number in the range of $2.2 \times 10^4 \leqslant Ra \leqslant 3.75 \times 10^4$, show that it goes from an oscillatory state up to chaos behavior.

## 5. Summary and conclusions

In this paper, the MHD natural convection in a LME was analyzed using the open source CFD library OpenFOAM. Through numerical simulations, the temperature, velocity, pressure, electric potential and induced electric currents fields were obtained. Conclusions are summarized as follow:

1. Natural convection in a LME displays the typical Bénard cells observed in similar configurations with other working fluids.
2. Velocity profiles for the case without current are in the same order of magnitude than those reported experimentally.
3. When a direct electrical current density is injected in the LME, two flow behaviors are observed: for the interval $0 < j_0 < 2750\ \mathrm{A\ m^{-2}}$ the velocity profiles are less curved than those without current, this is an indication that the flow is more ordered and represented by a small number of vortices and by smaller values of the $\overline{Nu}$ number than that for $j_0 = 0$; while for the $2750 \leqslant j_0 \leqslant 4000\ \mathrm{A\ m^{-2}}$ interval, velocity profiles with and without current are similar (for instance see profiles for $j_0 = 0$ and $j_0 = 3500\ \mathrm{A\ m^{-2}}$ in Fig. 14a) and the $\overline{Nu}$ number increases to reach almost the same value than that for $j_0 = 0$, a possible indication that ohmic heating also contributes to changes in the flow.
4. The $\overline{Nu}$ value for $j_0 = 0$ is quite similar to the one obtained by using a correlation for mercury reported in the literature. Furthermore, the observed *Nu* time evolution is in agreement with other experimental and numerical studies for liquid metals, where it goes from an oscillatory state up to chaos behavior.
5. In general, good qualitative agreement is observed between numerical and the reported experimental results for a LME configuration.

Although a more detailed exploration of the flow, thermal and MHD behavior is necessary, this study provides a theoretical basis for further research on the numerical simulation of MHD natural convection in LMBs. And based on the study in this paper, a more complicated configuration can be researched; for instance, to consider the temperature, electric potential and induced current distributions in the stainless steel cylindrical vessel.

## Acknowledgements

The author would like to acknowledge UNAM-DGAPA-PAPIIT for the financial support through Project IA102315.

## References

[1] R. Van Noorden, A better battery, Nature 507 (2) (2014).
[2] D.J. Bradwell, H. Kim, D.R. Sadoway, Magnesium-antimony liquid metal battery for stationary energy storage, J. Am. Chem. Soc. 134 (2012).
[3] H. Kim, D.A. Boysen, J.M. Newhouse, B.L. Spatocco, B. Chung, P.J. Burke, D.J. Bradwell, K. Jiang, A.A. Tomaszowska, K. Wang, W. Wei, L.A. Ortiz, S.A. Barriga, S.M. Poizeau, D.R. Sadoway, Liquid metal batteries: past, present, and future, Chem. Rev. 113 (3) (2013) 2075–2099.

[4] B. Arguss, Regenerative Battery, US Patent 3, 1966, p. 245,836.
[5] K. Wang, K. Jiang, B. Chung, T. Ouchi, P.J. Burke, D.A. Boysen, D.J. Bradwell, H. Kim, U. Muecke, D.R. Sadoway, Lithium-antimony-lead liquid metal battery for grid-level energy storage, Nature 514 (7522) (2014) 348–350.
[6] D.R. Sadoway, G. Ceder, D.J. Bradwell, High-amperage Energy Storage Device and Method, US Patent Application, US 2008/0044725 A1, 2008.
[7] D.R. Sadoway, Cost based discovery, Pan Eur. Networks: Sci. Technol. 12 (2014).
[8] R.J. Tayler, Hydromagnetic instabilities of an ideally conducting fluid, Proc. Phys. Soc. Sect. B 70 (1) (1957) 31.
[9] R.J. Tayler, Adiabatic stability of stars containing magnetic fields. 1-toroidal fields, Mon. Not. R. Astron. Soc. 161 (1973) 365.
[10] M. Seilmayer, F. Stefani, T. Gundrum, T. Weier, G. Gerbeth, M. Gellert, G. Rüdiger, Experimental evidence for a transient Tayler instability in a cylindrical liquid-metal column, Phys. Rev. Lett. 108 (2012) 244501.
[11] N. Weber, V. Galindo, F. Stefani, T. Weier, T. Wondrak, Numerical simulation of the Tayler instability in liquid metals, New J. Phys. 15 (4) (2013) 043034.
[12] A.D. Sneyd, Interfacial instabilities in aluminium reduction cells, J. Fluid Mech. 236 (3) (1992) 111–126.
[13] P.A. Davidson, R.I. Lindsay, Stability of interfacial waves in aluminium reduction cells, J. Fluid Mech. 362 (5) (1998) 273–295.
[14] P.A. Davidson, Overview overcoming instabilities in aluminium reduction cells: a route to cheaper aluminium, Mater. Sci. Technol. 16 (5) (2000) 475–479.
[15] D.H. Kelley, D.R. Sadoway, Mixing in a liquid metal electrode, Phys. Fluids 26 (5) (2014) 057102.
[16] OpenFOAM Foundation, 2012. <www.openfoam.org/>.
[17] S. Horanyi, L. Krebs, U. Müller, Turbulent Rayleigh-Bénard convection in low Prandtl-number fluids, Int. J. Heat Mass Transfer 42 (21) (1999) 3983–4003.
[18] R. Verzicco, R. Camussi, Transitional regimes of low-Prandtl thermal convection in a cylindrical cell, Phys. Fluids 9 (5) (1997) 1287–1295.